Research Square

Preprints are preliminary reports that have not undergone peer review.
They should not be considered conclusive, used to inform clinical practice,
or referenced by the media as validated information.

Seismic Response Mitigation in Wind Turbine Towers Using a nonlinear Magnetic Damper

Reza Pourjafar

rezpou@webmail.guilan.ac.ir

University of Guilan

Research Article

Keywords: Structural dynamics, Vibration control, Magnetic damper, Nonlinear absorber, Wind turbine tower, Seismic response

Posted Date: February 26th, 2026

DOI: https://doi.org/10.21203/rs.3.rs-8886132/v1

License: This work is licensed under a Creative Commons Attribution 4.0 International License.
Read Full License

Additional Declarations: No competing interests reported.

Seismic Response Mitigation in Wind Turbine Towers Using a nonlinear Magnetic Damper

Reza Pourjafar[1]

[1] Department of Civil Engineering, University of Guilan, Rasht, Iran.

Contact info:

Pourjafar R: rezpou@webmail.guilan.ac.ir (Corresponding author)

Abstract

Wind turbines in seismically active regions are increasingly vulnerable to earthquake-induced vibrations due to their growing height and flexibility. Effective vibration control is therefore essential to ensure structural safety and operational reliability. This study examines the performance of a novel magnetic damper in mitigating the seismic response of wind turbine towers. The tower is modeled through a three-degree-of-freedom modal representation, corresponding to the first three fore–aft mode shapes obtained from a finite element–based modal analysis. A synthetic acceleration record was then developed to represent the dynamic characteristics of five well-known earthquakes, providing a comprehensive excitation spectrum for evaluation. The damper parameters were optimized using a Bayesian optimization framework, with the root-mean-square of tower-top displacement adopted as the objective function. The optimized configuration was subsequently assessed under each individual earthquake record to evaluate its robustness. Results show that the proposed damper, together with the optimization scheme, achieves notable reductions in seismic response and maintains consistent performance across different ground motions. The findings demonstrate the effectiveness and adaptability of the magnetic damper in enhancing the seismic resilience of wind turbine structures and provide a promising direction for integrating smart damping technologies into renewable energy systems.

Keywords: Structural dynamics; Vibration control; Magnetic damper; Nonlinear absorber; Wind turbine tower; Seismic response.

Introduction

The rapid expansion of wind energy has led to the development of increasingly tall and flexible wind turbine towers, enabling higher power generation and improved energy capture. At the same time, the global spread of wind energy infrastructure means that an increasing number of turbines are being installed in regions with moderate to high earthquake hazard. This structural evolution, combined with exposure to seismically active environments, has made modern turbines more susceptible to dynamic excitations arising from wind, wave, and ground motion. Among these, earthquakes pose a unique challenge due to their broadband frequency content and unpredictable nature, which can induce significant lateral vibrations and threaten the structural integrity of turbine towers. Ensuring the seismic resilience of these large-scale structures is therefore essential for the reliability and safety of wind energy systems, particularly in seismically active regions.

Structural control methods have long been employed to mitigate dynamic loads on tall and slender structures while reducing the need for overly massive structural components. Among the various approaches developed, passive control systems have gained the widest acceptance due to their simplicity, cost-effectiveness, and reliability. Unlike active or semi-active devices, passive control mechanisms operate without external power, making them particularly attractive for applications such as wind turbine towers. Since the pioneering investigation of tuned mass dampers (TMDs) for wind turbines by Enevoldsen and Mørk (1996), numerous studies have explored and refined their use in this context. Notably, the works of Murtagh et al. (2008) and Stewart and Lackner (2013) advanced the understanding of TMD dynamics and performance under wind and wave excitations. More recently, efforts have focused on enhancing TMD efficiency through novel configurations and improved mechanical characteristics, reflecting a growing

research interest in advanced vibration control strategies for wind turbine applications (Zuo et al., 2020).

Several innovative passive control devices have been proposed to enhance the performance of conventional TMDs in wind turbine applications. Jahangiri and Sun (2018, 2020) introduced a three-dimensional pendulum TMD capable of bi-directional damping, outperforming dual TMD configurations installed along orthogonal directions (Stewart and Lackner, 2014; Tong et al., 2017; Zhao et al., 2018). This device, tuned to the first fore–aft natural frequency of the tower through gravitational effects, offers enhanced control efficiency but may face practical challenges due to the large pendulum length required for low-frequency tuning in nacelle installations. Traditional viscous dampers, commonly represented by dashpots in TMD models, also suffer from issues such as oil leakage, maintenance demands, and performance degradation (Wang et al., 2012). To address these drawbacks, Lian et al. (2018) proposed an eddy current TMD (EC-TMD) that employs relative motion between permanent magnets and a conductive plate, demonstrating effective vibration mitigation without physical contact. Other alternatives, such as ball vibration absorbers (BVAs) (Li et al., 2012; Zhang et al., 2013) and spherical BVAs (Chen and Georgakis, 2013), rely on frictional energy dissipation through rolling elements, though their tuning requirements often result in large geometries impractical for nacelle space. More recently, particle TMDs have shown promising robustness and broader effective frequency bandwidths (Lu et al., 2023; Zhao et al., 2024), particularly in attenuating higher vibration modes under seismic and aerodynamic excitations. To address the stroke limitations of conventional TMDs, Lin et al. (2024) developed a novel TMD configuration for floating wind turbine towers and demonstrated superior vibration suppression compared with traditional designs. Related studies on alternative damping concepts for offshore wind turbines have also been reported. Alotta et al. (2023) proposed a novel floating absorber for pitch motion mitigation of floating offshore wind turbines, highlighting that a key advantage of their device is that it does not need to be installed inside the nacelle, unlike conventional TMDs. Similarly, Tian et al. (2025) developed a new damping system for semi-submersible floating wind turbines and reported a significant reduction in fatigue damage when the device was employed.

Nonlinear dampers, offering a wider effective frequency range than their linear counterparts (Main and Jones, 2002), have attracted increasing attention as a means to overcome the inherent limitations of conventional linear devices. Jahangiri and Sun (2022) proposed a three-dimensional nonlinear TMD for vibration control of floating offshore wind turbines and reported that the device provided improved vibration mitigation compared to a linear TMD. The performance of a nonlinear TMD for wind turbine blades was also investigated in a later study (Jahangiri et al., 2024). Liu et al. (2023) examined the influence of modeling nonlinearities in a pendulum TMD with a prestressed cable and observed enhanced performance compared to the damper modeled with a linear cable. Magnetic forces naturally exhibit a strongly nonlinear force–displacement relationship, making magnet-based vibration dissipation devices inherently nonlinear. One of the earliest studies on magnetic vibration absorbers was conducted by Kojima and Nagaya (1985), who proposed a simple configuration consisting of a moving magnet positioned between two fixed repulsive magnets. Shi and Zhu (2015) investigated a negative-stiffness damper in which corrective forces from fixed magnets act on a central moving magnet. Benacchio et al. (2016) examined a tunable magnetic vibration absorber with adjustable linear and nonlinear stiffness parameters on a three-story structure, demonstrating that the device can function as a nonlinear energy sink, a nonlinear tuned vibration absorber, or a bi-stable absorber simply by altering the

magnetic and geometric properties of the magnets. Similarly, Feudo et al. (2018) reported that magnetic vibration absorbers are highly effective in controlling the first vibration mode, though some energy may be transferred to higher modes. These studies collectively highlight the versatility and potential of magnetic damping devices for structural vibration mitigation.

Pourjafar et al. (2025) recently proposed a novel magnetic damping device for vibration control of WTTs and demonstrated that it can achieve performance comparable to conventional linear TMDs while requiring significantly less installation space. Unlike pendulum-based TMDs, the proposed damper eliminates the need for long cables and, owing to its compact, box-like configuration, can also be conveniently mounted on top of the nacelle without occupying critical internal space. In the present study, the WTT is modeled using a three-degree-of-freedom (3-DOF) modal representation corresponding to the first three fore–aft mode shapes, obtained via finite element, with the damper introduced as an additional degree of freedom. The primary objective is to investigate the seismic response reduction achievable through the proposed device for WTTs. To this end, the damper parameters are optimized for a synthetic earthquake record constructed from five well-known ground motions, using a machine-learning-assisted Bayesian optimization framework. The study thereby is also meant to establish a general and efficient methodology for the optimal seismic design of the proposed nonlinear magnetic damper for wind turbine applications.

The scope of this work is limited to a numerical feasibility and performance assessment based on an idealized structural model. The wind turbine tower is represented as a linear cantilever structure with fore–aft bending modes only, while aerodynamic effects, soil–structure interaction, geometric and material nonlinearities of the tower, and experimental validation of the damper are not considered. Furthermore, the seismic optimization is performed using a single synthetic accelerogram intended to capture the average spectral characteristics of a selected set of earthquakes rather than to represent site-specific hazard conditions. These assumptions are adopted to focus on isolating the fundamental dynamic interaction between the tower and the nonlinear magnetic damper and to evaluate the effectiveness of the proposed optimization framework. Extension of the present methodology to higher-fidelity aero-servo-elastic models, multi-directional seismic excitation, and experimental validation constitutes important directions for future research.

2. Methodology

2.1 Tower model

The dynamic behavior of the DTU 10 MW reference wind turbine (RWT), schematically shown in Fig. 1, is described using a reduced-order modal formulation. The tower is idealized as a cantilever beam rigidly fixed at the base and carrying a lumped representation of the Rotor–Nacelle Assembly (RNA) at the tower top. The structural model includes three generalized modal coordinates associated with the first three fore–aft bending modes of the tower, along with an extra degree of freedom accounting for the relative motion of the damper. The tower natural frequencies and corresponding mode shapes, including the effects of the RNA mass and rotational inertia, were obtained using the finite-element-based code BModes (Bir, 2006). According to DTU Wind Energy Report I-0092, the fundamental fore–aft natural frequency of the 10 MW tower is 0.25 Hz (Bak et al., 2013), while the value computed in the present study is 0.26 Hz, demonstrating

acceptable agreement. A uniform modal damping ratio of 1% is assigned to all tower modes following the same DTU recommendations. The mode shapes adopted in the simulations are presented in Fig. 2. The nonlinear damper, introduced in the subsequent subsection, is installed at the tower top and dynamically interacts with the first three tower modes. Accordingly, the equations of motion for the coupled tower–damper system are formulated in modal coordinates as follows:

$$[M]\left[\ddot{X}\right] + [C]\left[\dot{X}\right] + [K][X] + [K_3][X_{d3}] + [K_5][X_{d5}] = [f_{EQ}(t)] \tag{1}$$

In the above formulation, $[M]$, $[C]$, and $[K]$ denote the modal mass, damping, and stiffness matrices, respectively, while $[X]$ and $[f_{EQ}]$ represent the generalized displacement and earthquake excitation, introduced as a base acceleration input multiplied by the generalized masses of each tower mode. The matrices $[K_3]$ and $[K_5]$, together with their associated displacement vectors, account for the higher-order nonlinear stiffness contributions of the damping device. Equation (1) is integrated numerically in the time domain using the Runge–Kutta–Nyström scheme. Accordingly, the generalized coordinate vector is defined as:

$$[X] = \begin{bmatrix} x_1 \\ x_2 \\ x_3 \\ x_d \end{bmatrix}, \quad [X_{d3}] = \begin{bmatrix} 0 \\ 0 \\ 0 \\ {x_d}^3 \end{bmatrix}, \quad [X_{d5}] = \begin{bmatrix} 0 \\ 0 \\ 0 \\ {x_d}^5 \end{bmatrix} \tag{2}$$

Here, x_d represents the generalized displacement of the damper, defined as the relative motion between the damper mass and the tower top node. The corresponding displacement at any point along the tower height is then given by:

$$u_x(x) = x_1\varphi_1(x) + x_2\varphi_2(x) + x_3\varphi_3(x) \tag{3}$$

where $\varphi_n(n = 1, \dots, 3)$ denote the tower mode shapes shown in Fig. 2. Detailed expressions for the mass, damping, and stiffness matrices are provided in the Appendix.

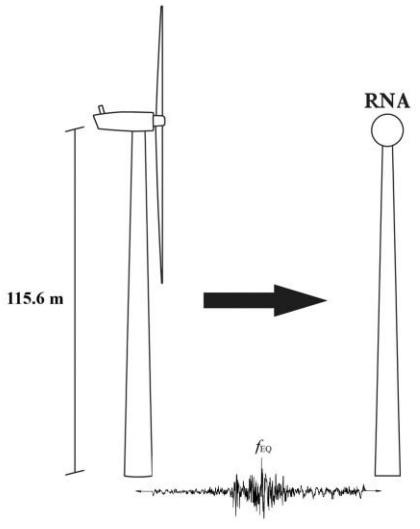


Figure 1. Schematic representation of DTU 10 MW WT and the equivalent tower model with the concentrated RNA at the top.

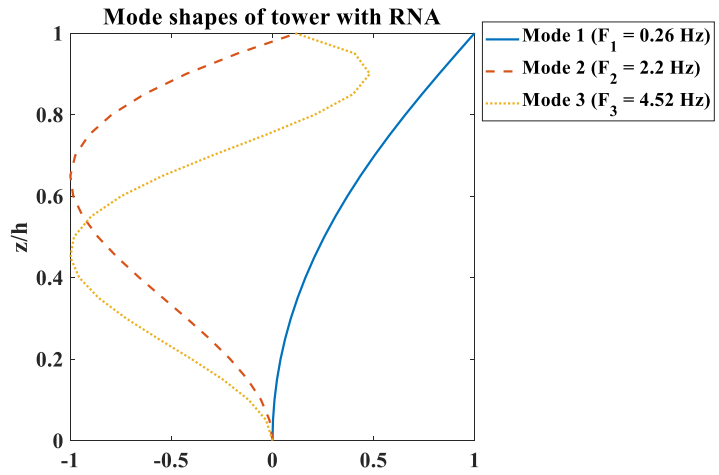


Figure 2. Normalized mode shapes of the tower with RNA mass and inertia at the top.

2.2 Bi-directional magnetic damper

The novel bi-directional magnetic damper is schematically shown in Fig. 3 (top view). The central magnets are fixed on a plate supported by rollers, allowing free movement in all directions (Rx = 0, Ry = 0; other reactions ≠ 0), while the side magnets are mounted on sliders that constrain motion to a single direction (either Rx = 0 or Ry = 0, Fig. 4). Telescopic joints with zero axial force (N = 0, M ≠ 0, V ≠ 0) connect the middle and side magnets, permitting axial displacement. The washer-shaped magnets are axially magnetized, and the layout ensures that the middle magnets remain aligned with the side magnets in each direction, producing repulsive forces that vary nonlinearly with relative displacement. Eddy current damping is achieved by placing copper plates along the sides of the damper box, against which the side magnets move. The relative motion induces a velocity-dependent damping force opposite to the motion, providing additional vibration dissipation. Together, the magnetic forces, eddy current damping, and the mass of 6 magnets, moving in each direction, replicate the functions of stiffness, damping, and mass in a traditional TMD. Thus, the device can be regarded as a nonlinear TMD with eddy current damping, with its primary distinction being the contactless, displacement-dependent magnetic forces.

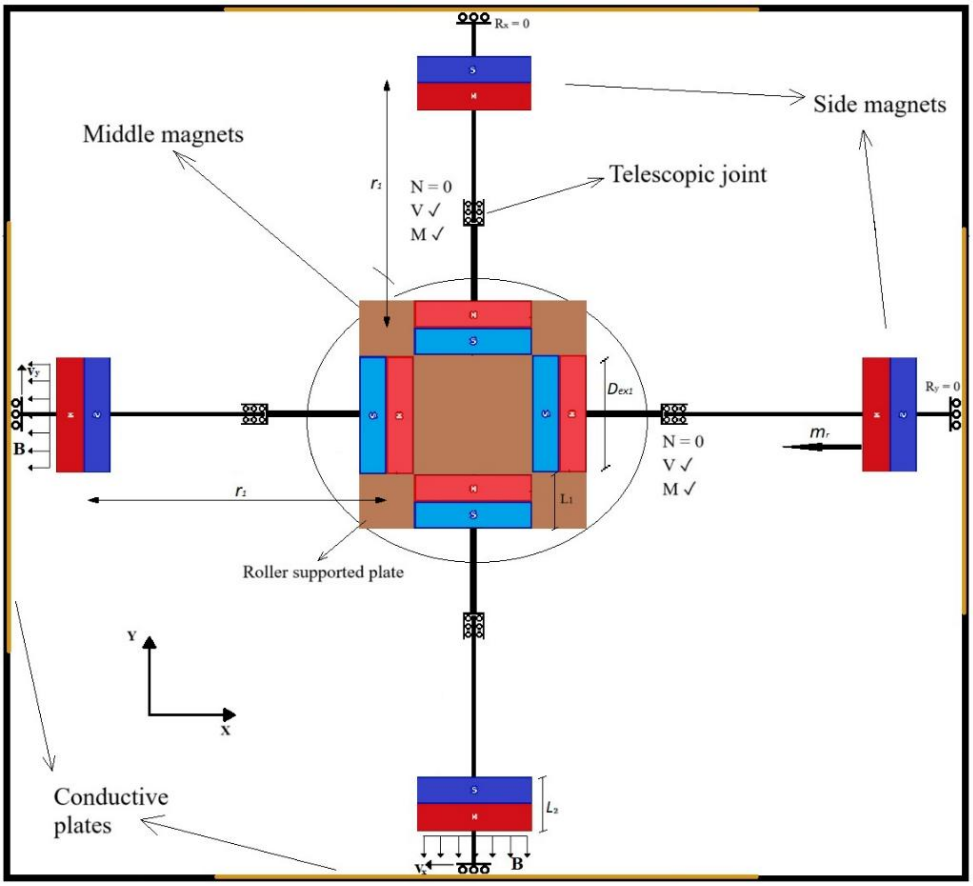


Figure 3. Two-dimensional schematic presentation of the proposed magnetic damper.

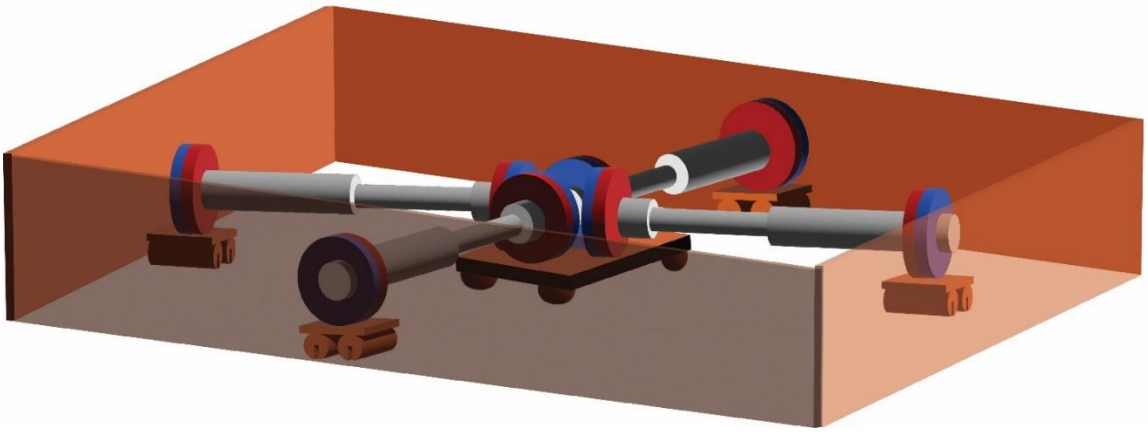


Figure 4. Three-dimensional schematic view of the magnetic damper.

Assuming displacement occurs only in the x-direction (tower fore–aft), the magnetic and eddy current damping forces are expressed as follows:

$$\boldsymbol{F}_{sx}(x) = -K_1 x - K_3 x^3 - K_5 x^5 \quad (4)$$

$$\boldsymbol{F}_{Dx}(v) = -2.\sigma.v.B^2.S.\delta \quad (5)$$

here, K_1, K_3, and $K_5$are defined in equations (6) – (8); v is the relative velocity; B is the magnetic flux density; and σ, V, S, and δdenote the electrical conductivity, volume, surface area, and thickness of the conductive plate, respectively.

$$K_1 = \frac{\mu_0 m_1}{2\pi}\left(\frac{24\, m_2}{{r_1}^5} + \frac{30L^2 A_3}{4\,{r_1}^7} + \frac{56L^4\, A_5}{16\,{r_1}^9} + \frac{90L^6\, A_7}{64\,{r_1}^{11}}\right) \quad (6)$$

$$K_3 = \frac{\mu_0 m_1}{2\pi}\left(\frac{120\, m_2}{{r_1}^7} + \frac{70L^2 A_3}{{r_1}^9} + \frac{105L^4\, A_5}{2\,{r_1}^{11}} + \frac{495L^6\, A_7}{16\,{r_1}^{13}}\right) \quad (7)$$

$$K_5 = \frac{\mu_0 m_1}{2\pi}\left(\frac{336\, m_2}{{r_1}^9} + \frac{315L^2 A_3}{{r_1}^{11}} + \frac{693L^4\, A_5}{2\,{r_1}^{13}} + \frac{9009L^6\, A_7}{32\,{r_1}^{15}}\right) \quad (8)$$

The magnetic dipole moments of the middle and side magnets, m_1 and m_2, are assumed equal in this study. μ_0 is the permeability of free space, r_1 is the initial distance between the magnet centers (assumed equal to r_2, see Fig. 3), and L is the magnet thickness.

$$A_3 = \left(4 - 3{\beta_{ex2}}^2\right)m_{ex2} - \left(4 - 3{\beta_{in1}}^2\right)m_{in1} \quad (9)$$

$$A_5 = \left(\frac{15{\beta_{ex2}}^4 - 60{\beta_{ex2}}^2 + 24}{4}\right)m_{ex2} - \left(\frac{15{\beta_{in2}}^4 - 60{\beta_{in2}}^2 + 24}{4}\right)m_{in2} \quad (10)$$

$$A_7 = \left(\frac{64 - 336{\beta_{ex2}}^2 + 280{\beta_{ex2}}^4 - 35{\beta_{ex2}}^6}{1024}\right)758 m_{ex2} - \left(\frac{64 - 336{\beta_{in2}}^2 + 280{\beta_{in2}}^4 - 35{\beta_{in2}}^6}{1024}\right)758 m_{in2} \quad (11)$$

The parameters β_{ex2} and β_{in2} represent the diameter-to-thickness ratios, while m_{ex2} and m_{in2} correspond to the dipole moments of the full and equivalent hole-size cylinder of the side magnets, respectively. More details on the derivation of the magnetic forces and eddy current damping are provided in Pourjafar et al. (2025).

2.3 Ground Motion Input

Structural seismic design and optimization are commonly performed using site-specific ground motion suites consistent with a target hazard level or conditional mean spectrum (Caicedo et al., 2024). In the present study, however, detailed seismic hazard characterization is beyond the scope. Instead, the focus is placed on assessing the effectiveness and robustness of the proposed Bayesian-based damper optimization framework. If the methodology exhibits consistent performance under a set of uncorrelated ground motions with distinct spectral and frequency characteristics, its effectiveness is expected to be even greater when applied to site-specific and spectrally correlated records. In this study a synthetic acceleration record is generated and scaled based on a suite of earthquake records.

Accordingly, five well-known earthquake records—Cape Mendocino (1992), Northridge (1994), Rudbar (1990), Kobe (1995), and Chi-Chi (1999)—were selected to construct a single

representative synthetic accelerogram. The main characteristics of the selected records are summarized in Table 1. All motions were baseline-corrected, band-pass filtered using a fourth-order Butterworth filter (0.1–24 Hz), resampled to a uniform time step of 0.01 s, and zero-padded to a common duration. This preprocessing ensured comparable frequency content and time length prior to spectral combination.

Let $a_i(t)$denote the filtered and aligned acceleration time histories of the five earthquakes, $i = 1, \dots, 5$. The Fast Fourier Transform (FFT) of each signal is given by:

$$A_i(f) = \mathcal{F}\{a_i(t)\} = | A_i(f) | e^{j\phi_i(f)} \tag{12}$$

where $| A_i(f) |$and $\phi_i(f)$ denote the amplitude and phase spectra of the i-th record, respectively. The mean amplitude spectrum of the selected ground motion set was computed as:

$$| A_{\text{avg}}(f) | = \frac{1}{5}\sum_{i=1}^{5} | A_i(f) | \tag{13}$$

The reference phase spectrum, $\phi_{\text{ref}}(f)$, was adopted from Rudbar earthquake record, as it provides a physically realistic phase distribution with minimal artificial discontinuities. The complex spectrum of the synthetic accelerogram was then constructed as:

$$A_{\text{syn}}(f) = | A_{\text{avg}}(f) | \ e^{j\phi_{\text{ref}}(f)} \tag{14}$$

The synthetic time history was subsequently obtained by applying the inverse Fourier Transform to the combined spectrum (Boore, 2003):

$$a_{\text{syn}}(t) = \mathcal{F}^{-1}\{A_{\text{syn}}(f)\} \tag{15}$$

The resulting acceleration signal, $a_{\text{syn}}(t)$, shown in Fig. 5, represents a synthetic earthquake record whose amplitude content captures the average frequency characteristics of the selected earthquakes, while its phase structure remains physically consistent and representative of real seismic excitations. The acceleration response spectrum of each record, their average, labeled "Target" and the synthetic record are presented in Fig. 6, demonstrating good agreement between the synthetic and target spectrum, specially in $0.2T_1 - 2T_1$ range, with T_1 denoting the first natural period of the tower.

The synthetic ground motion was then applied to the system as a base acceleration in the Eq. (1), yielding the seismic force vector,

$$f_{EQ}(t) = -a_{syn}(t)\begin{bmatrix} GM_1 \\ GM_2 \\ GM_3 \\ 0 \end{bmatrix} \tag{16}$$

where GM_n denotes the n-th generalized modal mass of the tower, as defined in Eq. (A.3). Since the fourth coordinate corresponds to the relative motion of the damper mass, the seismic excitation does not act directly on this degree of freedom, and the associated force component is therefore zero.

Table 1. Ground motion characteristics (PGA, duration, and energy content) of the selected earthquake records used to construct the representative synthetic excitation.

Earthquake	Area intensity (m/s)	PGA (m/s^2)	Duration (s)
Rudbar	5.27	6.09	50
Kobe	3.07	6.8	40
Cape Mendocino	5.8	14.6	30
Northridge	1.5226	3.3749	40
Chi-Chi	6.9542	8.7481	60

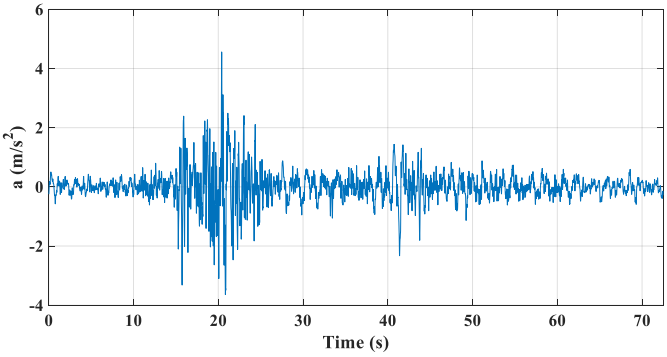


Figure 5. Generated synthetic accelerogram.

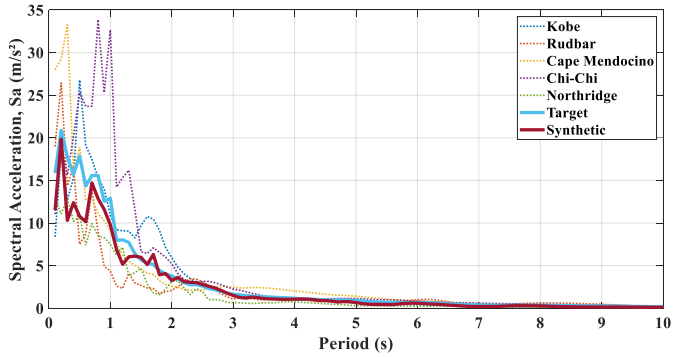


Figure 6. Acceleration response spectra of the five recorded ground motions, their averaged target spectrum, and the spectrum of the generated synthetic record.

2.4 Bayesian optimization

Considering the number of optimizable parameters associated with the magnetic damper, an exhaustive numerical grid-search optimization would be computationally prohibitive (Pourjafar and Razzaghi, 2025). Therefore, Bayesian optimization (BO), a surrogate-assisted global optimization technique, is adopted in this study. BO is a sample-efficient framework for minimizing computationally expensive black-box functions where gradient information is unavailable (Garnett, 2023). It constructs a probabilistic surrogate of the objective function and sequentially selects new evaluation points by balancing exploration of uncertain regions and exploitation of promising areas. In this study, a Gaussian Process (GP) is adopted as the surrogate model, which defines a distribution over functions as (Rasmussen and Williams, 2006)

$$f(\boldsymbol{p}) \sim \mathcal{GP}(m(\boldsymbol{p}), k(\boldsymbol{p}, \boldsymbol{p}')) \tag{17}$$

where $m(p)$ is the prior mean (commonly zero) and $k(p, p')$ is the covariance kernel (e.g., squared-exponential or Matérn). The GP posterior is updated using previously evaluated data, and new sampling points are determined by maximizing an acquisition function that quantifies the expected improvement over the current best observation. This approach efficiently guides the search toward the global optimum with far fewer function evaluations than population-based algorithms like Genetic Algorithm and Particle Swarm Optimization, making it well suited for optimization of computationally demanding structural dynamics problems.

In this study, the optimization vector is defined as $\mathbf{p} = [D_{\text{ex}},\ D_{\text{in}},\ L,\ B_r,\ r_1,\ \zeta]$, where D_{ex}, D_{in}, L, r_1, and B_r denote the magnets' external diameter, internal diameter, thickness, initial center-to-center gap between the magnets, and residual flux density, respectively. Here, ζrepresents the damping ratio of an equivalent linear damper. Since the parameters governing the nonlinear magnetic stiffness also influence the eddy current damping, directly optimizing both effects simultaneously would lead to coupled design variables. To decouple these two mechanisms and simplify the optimization process, viscous damping of a linear damper is assumed, and the eddy current damping is subsequently adjusted through the physical parameters σ, S, and δ in Eq. (5), which represent the electrical conductivity, surface area, and thickness of the conductive plate, respectively. The objective function $f(\mathbf{p})$ is defined as the root mean square (RMS) of the tower-top displacement.

The optimization of the magnetic damper parameters was carried out using a Bayesian optimization framework implemented through the bayesopt function in MATLAB. An expected-improvement acquisition function was adopted to balance global exploration and local exploitation, while the objective function was treated as deterministic. Parallel evaluations were enabled using the clipped-model-prediction strategy to enhance computational efficiency. A maximum of 200 objective function evaluations was allowed, with 50 initial seed points used to construct the initial surrogate model. To ensure physically meaningful and practically feasible solutions, explicit constraints were imposed on the design variables, including geometric admissibility conditions, upper bounds on admissible mass ratios, and limits on the initial separation distance between the magnets. These constraints guided the optimization toward realistic damper configurations without compromising the generality of the framework. A flowchart of the BO optimization procedure is presented in Fig. 7.

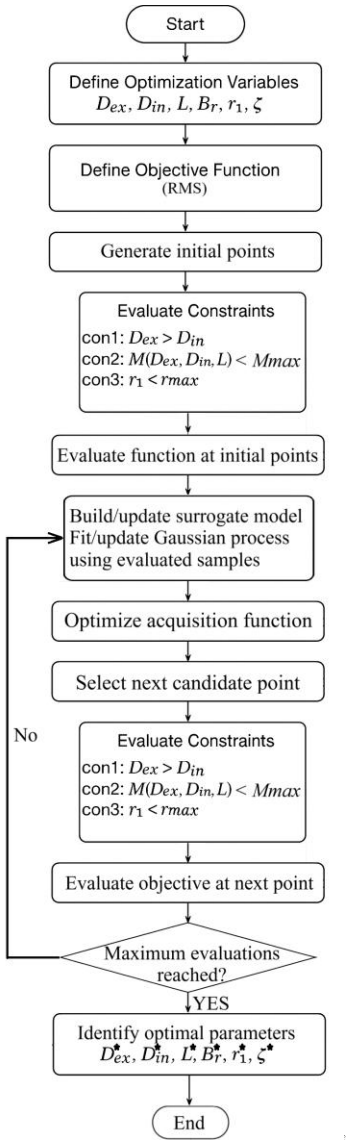


Figure 7. Flowchart of the magnetic damper Bayesian optimization.

3. Results and discussion

The nonlinear magnetic damper, together with the integrated design framework—comprising synthetic ground motion generation, Bayesian parameter optimization, and seismic response evaluation—proved highly effective in mitigating the tower-top displacement response. The optimized configurations demonstrate consistent improvement across all prescribed mass ratios, highlighting the robustness of the optimization framework and the adaptability of the proposed device. As illustrated in Fig. 8, the tower-top displacement time histories reveal a visibly lower oscillation amplitude when the optimized damper is engaged, confirming its strong capacity for vibration suppression under seismic loading. The corresponding displacement power spectral density (PSD) in Fig. 9 shows a pronounced attenuation of vibration energy around the tower's first natural frequency (0.26 Hz), indicating effective frequency tuning and efficient energy

transfer from the primary structure to the damper. This reduction is especially evident near resonance, where the uncontrolled response would otherwise be dominated by the fundamental mode.

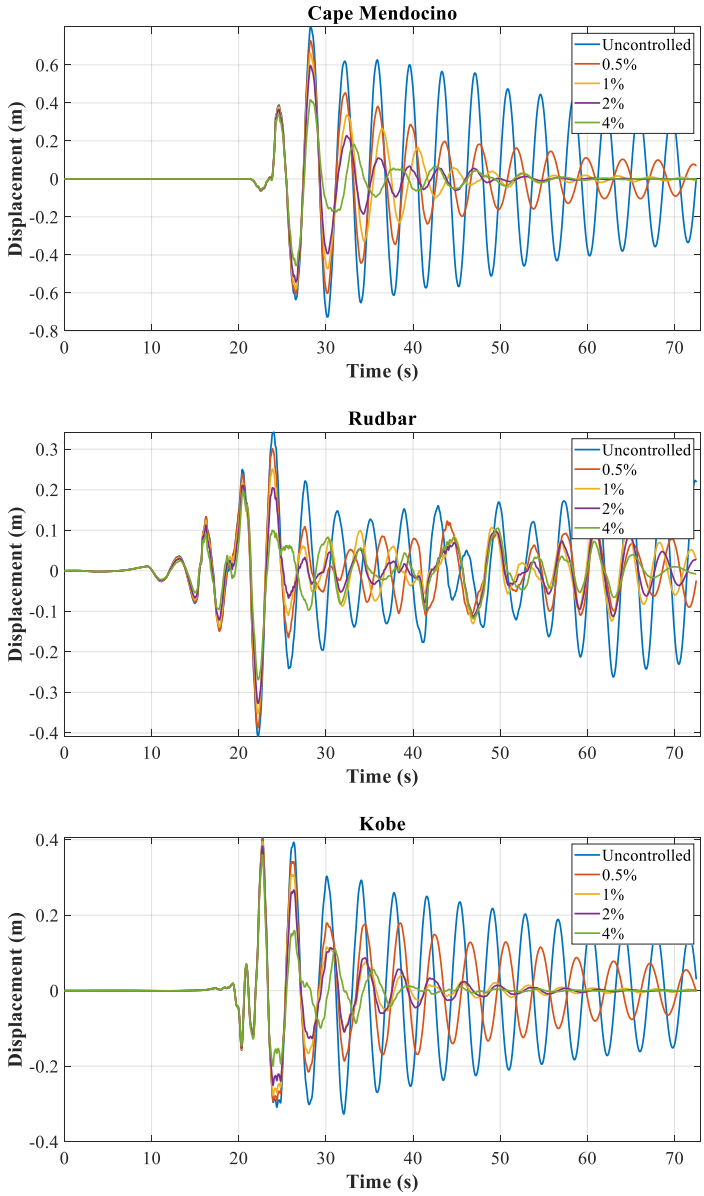


Figure 8. Tower-top displacement time histories of the uncontrolled and controlled cases under each earthquake excitation.

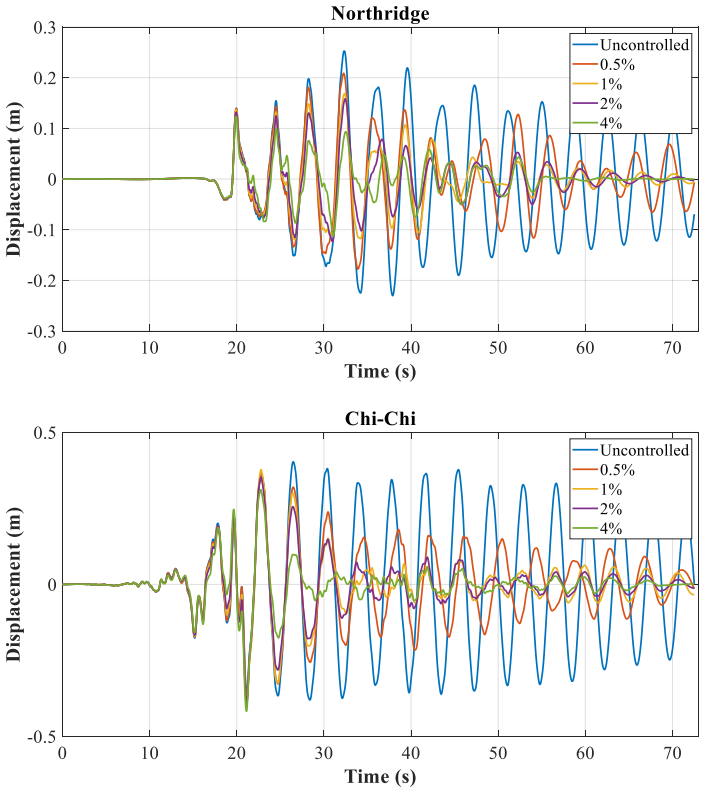


Figure 8 (Continued).

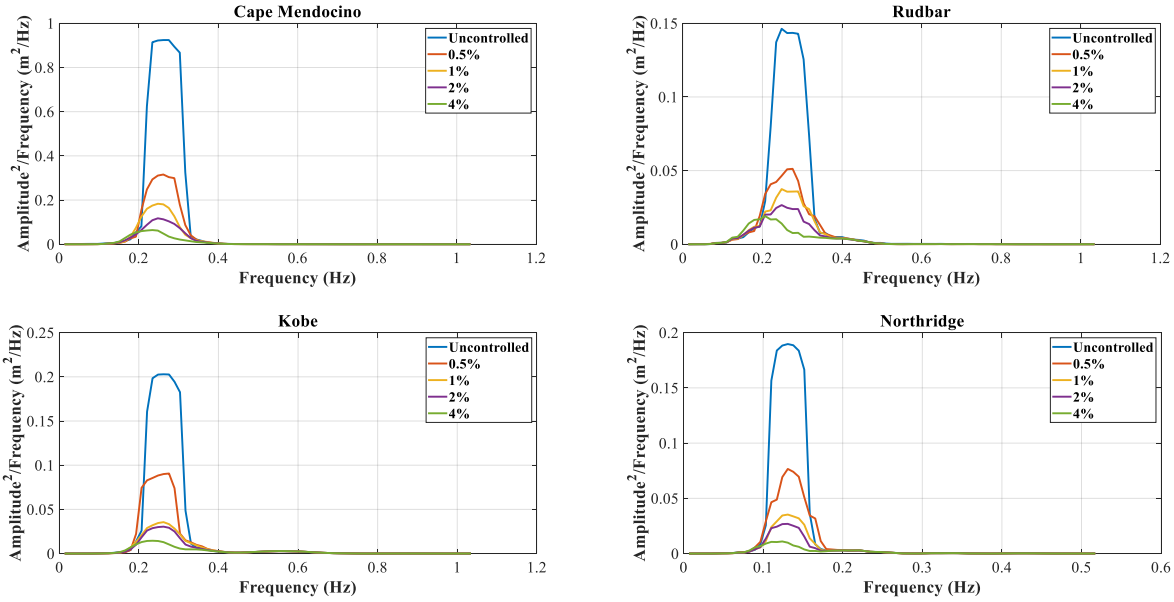


Figure 9. Power spectral density (PSD) of tower-top displacement due to each excitation record.

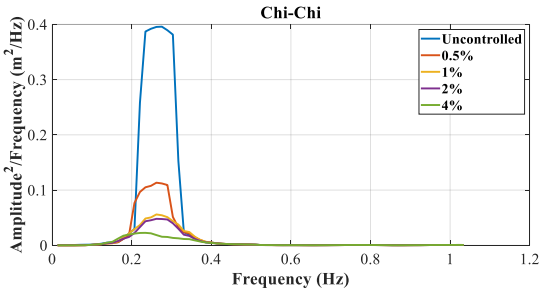


Figure 9 (Continued).

Fig. 10 compares the normalized RMS tower-top displacements, calculated relative to the uncontrolled case, for different damper mass ratios under the five earthquake records. The results reveal remarkably consistent reductions across all excitations, demonstrating that the proposed magnetic damper performs reliably regardless of the input ground motion characteristics. Averaged across all records, RMS reductions of approximately 36–65% are achieved for mass ratios ranging from 0.5% to 4%, confirming the scalability and effectiveness of the device. Although minor variations appear among records, the overall reduction trend remains uniform, underscoring the damper's robustness and stable energy dissipation capacity under diverse seismic excitations. This consistent performance indicates that the nonlinear magnetic damper maintains effective tuning and energy transfer even when the excitation intensity and frequency content vary substantially.

The BO framework demonstrated remarkable efficiency in tuning the six nonlinear damper parameters that govern the device's behavior. A conventional numerical grid search would have required millions of function evaluations even within moderate parameter bounds and step intervals, whereas BO achieved convergence after roughly 100 function calls, with minimal improvement between 100 to 200 evaluations. This highlights BO's strong capability to explore complex, high-dimensional design spaces with a fraction of the computational cost, proving its potential as a practical optimization tool for nonlinear damping systems.

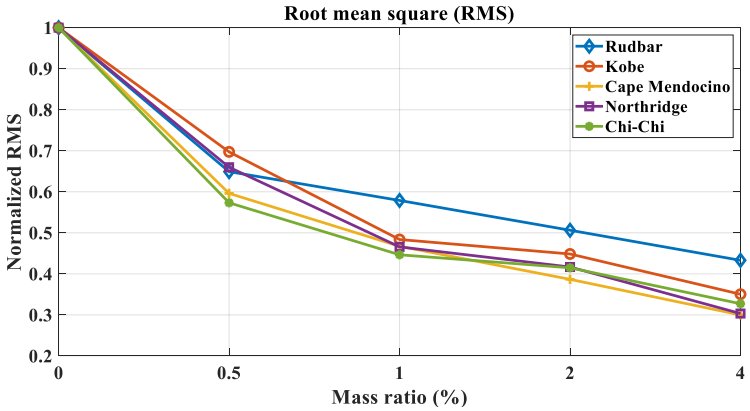


Figure 10. Normalized RMS of tower-top displacement for different damper-to-structure mass ratios under the five earthquake records.

Overall, the results confirm that the proposed nonlinear magnetic damper provides a robust and broadband solution for seismic vibration control of WTTs. Its compact, contact-free configuration makes it suitable for nacelle-top installation where space is limited. The optimized parameters obtained through Bayesian learning deliver consistent performance across all earthquake records,

validating both the reliability of the design methodology and the adaptability of the damper. The corresponding optimal parameters are presented in Table 2.

Table 2. Optimized parameters of the nonlinear magnetic damper obtained from Bayesian optimization for different damper-to-structure mass ratios.

Mass ratio (%) \ parameter	D_{ex} (m)	D_{in} (m)	L (m)	B_r (T)	r_1 (m)	ζ
0.5	0.692	0.465	0.64	1.049	1.45	0.02
1	1.031	0.404	0.366	1.221	1.55	0.13
2	1.307	0.519	0.495	1.022	1.66	0.267
4	1.659	0.757	0.64	1.345	1.951	0.283

Conclusion

This study examined the seismic performance of a nonlinear magnetic damper developed for vibration control of wind turbine towers. The damper was optimized using Bayesian optimization for a synthetic acceleration record representing the combined spectral characteristics of five well-known earthquake records, and the resulting configurations were subsequently evaluated under each record individually. This integrated framework—comprising synthetic ground motion generation, machine-learning-assisted optimization, and seismic response evaluation—proved highly effective in mitigating tower vibrations. The designed magnetic damper achieved 36–65% reductions in RMS tower-top displacement across all earthquake records, demonstrating strong vibration suppression and robust performance under varying seismic inputs. These results confirm the effectiveness and adaptability of the proposed magnetic damper in enhancing the seismic resilience of flexible tower structures.

The non-contact magnetic mechanism and nonlinear force characteristics of the damper enable broadband energy dissipation and amplitude-dependent adaptability, while its compact, flat geometry makes it suitable for nacelle-top installation without occupying internal space. Furthermore, the study highlights Bayesian optimization as an efficient and reliable approach for high-dimensional nonlinear design problems, achieving convergence with only about a hundred simulations. Collectively, the findings establish the nonlinear magnetic damper as a practical and scalable solution for improving the seismic performance of wind turbine towers.

Future work will extend the present study to higher-fidelity wind turbine models coupled with the proposed damper under combined environmental loading, including wind, wave, and multi-directional seismic excitations.

Appendix

The Mass, stiffness and damping matrices, presented in equation (1) are defined as follows,

$$[M] = \begin{bmatrix} M_{11} & M_{12} & M_{13} & M_{14} \\ M_{21} & M_{22} & M_{23} & M_{24} \\ M_{31} & M_{32} & M_{33} & M_{34} \\ M_{41} & M_{42} & M_{43} & M_{44} \end{bmatrix} \quad , \quad [C] = \begin{bmatrix} C_1 & 0 & 0 & 0 \\ 0 & C_2 & 0 & 0 \\ 0 & 0 & C_3 & 0 \\ 0 & 0 & 0 & C_d \end{bmatrix}$$

$$, \quad [K] = \begin{bmatrix} k_1 & 0 & 0 & 0 \\ 0 & k_2 & 0 & 0 \\ 0 & 0 & k_3 & 0 \\ 0 & 0 & 0 & K_d \end{bmatrix} \tag{A.1}$$

Where

$$M_{11} = GM_1 + M_d \cdot {\varphi_1}^2(h)$$
$$M_{12} = M_{21} = M_d \cdot \varphi_1(h) \cdot \varphi_2(h)$$
$$M_{13} = M_{31} = M_d \cdot \varphi_1(h) \cdot \varphi_3(h)$$
$$M_{14} = M_{41} = M_d \cdot \varphi_1(h)$$
$$M_{22} = GM_2 + M_d \cdot {\varphi_2}^2(h)$$
$$M_{23} = M_{32} = M_d \cdot \varphi_2(h) \cdot \varphi_3(h)$$
$$M_{24} = M_{42} = M_d \cdot \varphi_2(h)$$
$$M_{33} = GM_3 + M_d \cdot {\varphi_3}^2(h)$$
$$M_{34} = M_{43} = M_d \cdot \varphi_3(h)$$
$$M_{44} = M_d \tag{A.2}$$

In which,

$$GM_n = \int_0^h \varphi_n(x) \cdot m(x) \cdot \varphi_n(x)\, dx \quad , \quad n = 1, \dots, 3 \tag{A.3}$$

And

$$k_n = {\omega_n}^2 \cdot GM_n \tag{A.4}$$

$$C_n = 2 \cdot GM_n \cdot \omega_n \cdot \zeta_n \tag{A.5}$$

Funding sources

This research did not receive any specific grant from funding agencies in the public, commercial, or not-for-profit sectors.

Declaration of conflicting interest

On behalf of all authors, the corresponding author states that there is no conflict of interest.

Ethics, Consent to Participate, and Consent to Publish declarations:

Not applicable.

Data availability statement

The datasets generated during and/or analyzed during the current study are available from the corresponding author on reasonable request.

Author contributions

Reza Pourjafar: Conceptualization, Methodology, Software, Formal analysis, Investigation, Writing - Original Draft, Visualization.

References

Alotta G, Laface V, Faill G, Ruzzo C and Arena F (2023) A novel concept of floating absorber for motion mitigation in floating offshore wind turbines. *Engineering Structures*, 294, 116554. https://doi.org/10.1016/j.engstruct.2023.116554

Bak, C., Zahle, F., Bitsche, R., Kim, T., Yde, A., Henriksen, L.C., et al., 2013. The DTU 10-MW Reference Wind Turbine. J. Wind Energy. https://orbit.dtu.dk/en/publications/the-dtu-10-mw-reference-wind-turbine

Benacchio S, Malher A, Boisson J, Touzé C (2016) Design of a magnetic vibration absorber with tunable stiffnesses. Nonlinear Dynamics. 85. https://doi.org/10.1007/s11071-016-2731-3

Bir, G., 2006. User's Guide to BModes (Software for Computing Rotating Beam-Coupled Modes). NREL/TP-500-39133. http://dx.doi.org/10.2172/861489

Caicedo D, Karimzadeh S, Bernardo V and Lourenço PB (2024) Selection and Scaling Approaches of Earthquake Time-Series for Structural Engineering Applications: A State-of-the-Art Review. Arch Computat Methods Eng **31**, 1475–1505. https://doi.org/10.1007/s11831-023-10025-y

Chen J, Georgakis CT (2013) Tuned rolling-ball dampers for vibration control in wind turbines. J Sound Vib; 332:5271–82. https://doi.org/10.1016/j.jsv.2013.05.019

Enevoldsen, I., Mørk, K., 1996. Effects of a vibration mass damper in a wind turbine tower. J. Struct. Mech. 24, 155–187. http://dx.doi.org/10.1080/08905459608905260

Feudo L S, Touzé C, Boisson J, Cumunel G. (2018) Nonlinear magnetic vibration absorber for passive control of a multi–storey structure. Journal of Sound and Vibration. 438. https://doi.org/10.1016/j.jsv.2018.09.007

Garnett R (2023) Bayesian Optimization, Cambridge University Press. https://doi.org/10.1017/9781108348973

Jahangiri V & Sun C (2022) A novel three dimensional nonlinear tuned mass damper and its application in floating offshore wind turbines. Ocean Engineering, 250, 110703. https://doi.org/10.1016/j.oceaneng.2022.110703

Jahangiri V, Sun C and Babaei H (2024) Application of a new two dimensional nonlinear tuned mass damper in bi-directional vibration mitigation of wind turbine blades. Engineering Structures, 302, 117371. https://doi.org/10.1016/j.engstruct.2023.117371

Jahangiri, V., Sun, C., 2020. Three-dimensional vibration control of offshore floating wind turbines using multiple tuned mass dampers. Ocean Eng. 206, 107196. https://doi.org/10.1016/j.oceaneng.2020.107196

Kojima H, Nagaya K (1985) Forced vibrations of a circular plate with a nonlinear dynamic vibration absorber. Bull. JSME 28(136), 309–314.

Li J, Zhang Z, Chen J (2012) Experimental study on vibration control of offshore wind turbines using a ball vibration absorber. Energy Power Eng; 4:153–7. http://dx.doi.org/10.4236/epe.2012.43021

Lian J, Zhao Y, Lian C, Wang H, Dong X, Jiang Q, Zhou H, Jiang J (2018) Application of an eddy current-tuned mass damper to vibration mitigation of offshore wind turbines. Energies; 11:3319. https://doi.org/10.3390/en11123319

Lin J, Wang Y, Zhang G, Liu Y and Zhang J (2024) Novel tuned mass dampers installed inside tower of spar offshore floating wind turbines. Ocean Engineering, 301, 117412. https://doi.org/10.1016/j.oceaneng.2024.117412

Liu G, Lei Z, Law SS and Yang Q (2023) The nonlinear behavior of prestressed tuned mass damper for vibration control of wind turbine towers. *Nonlinear Dyn* 111, 10939–10955. https://doi.org/10.1007/s11071-023-08434-6

Lu Z, Zhao S, Ma C, Dai K (2023) Experimental and analytical study on the performance of wind turbine tower attached with particle tuned mass damper. Engineering Structures. 294. 116784. https://doi.org/10.1016/j.engstruct.2023.116784

Main JA, Jones NP (2002) Free vibrations of taut cable with attached damper II: nonlinear damper, J. Eng. Mech. 128 (10) 1072e1081.https://doi.org/10.1061/(ASCE)0733-9399(2002)128:10(1072)

Murtagh, P.J., Ghosh, A., Basu, B., Broderick, B.M., 2008. Passive control of wind turbine vibrations including blade/tower interaction and rotationally sampled turbulence. Wind Energy 11, 305–317. https://doi.org/10.1002/we.249

Pourjafar P and Razzaghi P (2025) Performance of a nonlinear tuned mass damper in structural vibration control of multi degree of freedom systems. Asian Journal of Civil Engineering. Epub ahead of print 22 September 2025. https://doi.org/10.21203/rs.3.rs-7480797/v1

Pourjafar R, Hansen MOL and Razzaghi J (2025) Passive control of wind turbine tower using nonlinear magnetic vibration absorber and eddy current damping. Wind Engineering. https://doi.org/10.1177/0309524X251317514

Rasmussen CE, Williams CKI (2003) Gaussian processes in machine learning. In *Summer school on machine learning*, pp. 63-71

Shi X, Zhu S (2015) Magnetic negative stiffness dampers. Smart Materials and Structures. 24. 10.1088/0964-1726/24/7/072002.

Stewart GM, Lackner MA (2014) The impact of passive tuned mass dampers and wind-wave misalignment on offshore wind turbine loads. Eng Struct; 73:54–61. https://doi.org/10.1016/j.engstruct.2014.04.045

Stewart, G., Lackner, M., 2013. Offshore wind turbine load reduction employing optimal passive tuned mass damping systems. IEEE Trans. Control Syst. Technol. 21, 1090–1104. http://dx.doi.org/10.1109/TCST.2013.2260825

Sun, C., Jahangiri, V., 2018. Bi-directional vibration control of offshore wind turbines using a 3D pendulum tuned mass damper. Mech. Syst. Signal Process. 105, 338–360. https://doi.org/10.1016/j.ymssp.2017.12.011

Tian H, Soltani MN, Yeter B and Galván-Pozos DE (2025) Design of a novel tower damping system for semi-submersible floating offshore wind turbines considering fatigue and ultimate limit states. Ocean Engineering, 320, 120343. https://doi.org/10.1016/j.oceaneng.2025.120343

Tong X, Zhao X, Zhao S (2015) Passive structural vibration control of a monopile wind turbine tower. In Proceedings of the 2015 54th IEEE Conference on Decision and Control (CDC), Osaka, Japan, 15–18 December; pp. 1352–1357. https://doi.org/10.1109/CDC.2015.7402399

Wang, Z, Chen, Z, Wang J (2012) Feasibility study of a large-scale tuned mass damper with eddy current damping mechanism. Earthq. Eng. Eng. Vib., 11, 391–401. https://doi.org/10.1007/s11803-012-0129-x

Zhang Z, Chen J, Li J (2013) Theoretical study and experimental verification of vibration control of offshore wind turbines by a ball vibration absorber. Struct Infrastruct Eng; 10:1087–100. https://doi.org/10.1080/15732479.2013.792098

Zhao B, Gao H, Wang Z, Lu Z (2018) Shaking table test on vibration control effects of a monopile offshore wind turbine with a tuned mass damper. Wind Energy;21 (12):1309–28. https://doi.org/10.1002/we.2256

Zhao S, Lu Z, Fan Q, Dai K (2024) Vibration Control Effect Analysis of PTMD in Wind Turbine Tower Under Multi-Hazard Action of Earthquake and Vortex-Induced Wind. Int J Struct Stab Dyn (2024), Article 2550021, https://doi.org/10.1142/S021945542550021X

Zuo, H., Bi, K., Hao, H., 2020. A state-of-the-art review on the vibration mitigation of wind turbines. Renew. Sustain. Energy Rev. 121, 109710. https://doi.org/10.1016/j.rser.2020.109710